Revision 1

Word count: 4702

Synthesis and structure analysis of $CaFe_2O_4$-type single crystals in the $NaAlSiO_4$-$MgAl_2O_4$-Fe_3O_4 system

Takayuki Ishii[*,1], Giacomo Criniti[2], Xiaoyu Wang[2], Konstantin Glazyrin[3], Tiziana Boffa Ballaran[2]

[1]Center for High Pressure Science and Technology Advanced Research, Beijing, 100094, China

[2]Bayerisches Geoinstitut, University of Bayreuth, 95440 Bayreuth, Germany

[3]Deutsches Elektronen-Synchrotron DESY, Notkestr. 85, 22607 Hamburg, Germany

ABSTRACT

Orthorhombic $CaFe_2O_4$-structured (Cf) Na-rich aluminous silicate (space group *Pbnm*) is a major mineral of metabasaltic rocks at lower mantle conditions and can therefore significantly affect the physical properties of subducted oceanic crusts. We attempted to synthesize single crystals of Cf-type phases in the systems $NaAlSiO_4$, $NaAlSiO_4$-$MgAl_2O_4$, $NaAlSiO_4$-$MgAl_2O_4$-Fe_3O_4, and $NaAlSiO_4$-$MgAl_2O_4$-Fe_3O_4-H_2O at 23-26 GPa and 1100-2200 °C. Under dry conditions, single-crystals of Cf-type phase up to 100-150 μm in size were recovered from 23 GPa and 2000-2200 °C. Single-crystal X-ray diffraction and composition analyses suggest that the synthesized Cf-type phases have few percent of vacancies in the 8-fold coordinated site with Na, Mg, and Fe^{2+} and partially disordered Al and Si in the octahedral sites. Iron-bearing Cf-type phases have 32-34% Fe^{3+} that is hosted both in the octahedral sites and in the 8-fold coordinated site. In $NaAlSiO_4$-$MgAl_2O_4$-Fe_3O_4-H_2O system, no formation of Cf-type phase was observed at 24 GPa and 1100-2000 °C, due to formation of hydrous Na-rich melt and Al-rich oxides or hydroxides, suggesting possible absence of Cf-type phase in hydrous basaltic crust. The single crystal syntheses of Cf-type phases will be useful to investigate their physical properties, improving models of lower mantle structure and dynamics.

Keywords: calcium ferrite, single crystal, multi-anvil press, high pressure, basaltic crust

INTRODUCTION

This is the peer-reviewed, final accepted version for American Mineralogist, published by the Mineralogical Society of America.
The published version is subject to change. Cite as Authors (Year) Title. American Mineralogist, in press.
DOI: https://doi.org/10.2138/am-2022-8748. http://www.minsocam.org/

$CaFe_2O_4$-type (Cf) phase is a major mineral phase (~25% in volume fraction) of subducted basaltic crusts at lower mantle conditions (e.g. Ishii et al. 2019a; 2022). The chemical formula of Cf-type phases is generally expressed as $A^{2+}B^{3+}{}_2O_4$ or $X^+(Y^{3+}Z^{4+})O_4$. The Cf structure is orthorhombic (space group *Pbnm*) and consists of double chains of edge-sharing $B^{3+}O_6$ or $(Y^{3+},Z^{4+})O_6$ octahedra running parallel to the *c*-axis of the unit cell. The octahedral double chains are linked to one another by sharing vertices and form channel-like cavities that extend parallel to the *c*-axis where relatively large A^{2+} or X^+ cations are accommodated (Yamada et al. 1983; Ishii et al. 2018). In a basaltic crust composition, Cf-type phases are constituted by a solid solution approximately expressed by the end members $NaAlSiO_4$, $MgAl_2O_4$, $FeAl_2O_4$ and Fe_3O_4.

Recent seismological and geodynamic studies suggest that significant amounts of basaltic crusts have been subducted and accumulated in the lower mantle (e.g., Kaneshima, 2019; Ballmer et al. 2015), stressing the importance of determining the chemical and physical properties of the Cf phase for better understanding of the lower-mantle structure and dynamics. Experimental studies of physical properties of single-crystal samples generally provide more information than those of polycrystalline aggregates because they allow to constrain the anisotropic properties of the material of interest. For instance, relatively large single crystals (>~100 μm) of high quality are required to determine physical properties such as the full elastic tensor, sound wave velocities anisotropy and thermal conductivity (e.g. Hsieh et al., 2020, 2022; Satta et al. 2021). To date, the structural and physical properties of Cf-type phase have been poorly constrained as measurements were conducted in limited systems and using polycrystalline samples.

Additionally, defects in minerals can significantly affect their transport properties such as electrical conductivity and viscosity because these properties are controlled through defects. Because of the large fraction of Cf phase in basaltic crusts, defect chemistry of Cf phase can play an important role in understanding physical properties of lower-mantle basaltic crusts and therefore the lower-mantle structure and dynamics. It has been suggested that Cf phase may have A-site vacancies based on electron microprobe analysis (e.g. Ono et al. 2009; Wu et al.

2017). Due to difficulty in accurately determining Na content by electron microprobe due to its volatilization during measurement, it is still under debate whether Cf phase has vacancies.

In this study, we attempted to synthesize large single crystals of Cf-type phase in the systems $NaAlSiO_4$, $NaAlSiO_4$-$MgAl_2O_4$, $NaAlSiO_4$-$MgAl_2O_4$-Fe_3O_4 and $NaAlSiO_4$-$MgAl_2O_4$-Fe_3O_4-H_2O at 23-26 GPa up to 2000-2200 °C by high pressure-temperature experiments. Single crystals of Cf-type phases with dimensions up to 150 μm were recovered in the dry systems and characterized by electron microprobe, Mössbauer spectroscopy and X-ray structural refinements. We examined their vacancy concentrations combining electron microprobe measurements and single crystal structural refinements of high-quality single crystals. Based on these results, we discuss the crystal chemistry, molar volume systematics and stability of Cf-type phase in a subducted basaltic crust.

EXPERIMENTAL METHODS

We prepared starting powders with $NaAlSiO_4$, 80 mol% $NaAlSiO_4$-20 mol% $MgAl_2O_4$, and 70 mol% $NaAlSiO_4$-20 mol% $MgAl_2O_4$-10 mol% Fe_3O_4 compositions using synthetic $NaAlSiO_4$ nepheline and $MgAl_2O_4$ spinel and reagent grade Fe_3O_4 magnetite. Synthetic $NaAlSiO_4$ nepheline was synthesized in a furnace using a mixture of Na_2CO_3, Al_2O_3 and SiO_2 with molar ratios 1.02:1:2, where the excess Na_2CO_3 was needed to balance Na evaporation at high temperature, following the procedure reported by Ono et al. (2009). $MgAl_2O_4$ spinel was obtained by heating a mixture of reagent grade MgO and Al_2O_3 with 1:1 molar ratio in a furnace at 1500 °C for 12 h. A hydrous mixture of 70 mol% $NaAlSiO_4$-20 mol% $MgAl_2O_4$-10 mol% Fe_3O_4 + ~11 wt.%H_2O composition was also prepared using reagent grade Na_2SiO_3, Fe_3O_4, SiO_2, $Al(OH)_3$ and synthetic $MgAl_2O_4$.

High pressure-temperature experiments were performed at 23-24 GPa and 1100-2200 °C for 2-5 h using 10-MN and 12-MN Kawai-type multi-anvil presses with a split-sphere-type guide block installed at the Bayerisches Geoinstitut, University of Bayreuth. A synthesis experiment using $NaAlSiO_4$ as starting composition was conducted at 26 GPa and 1700 °C using the 15-MN Kawai-type multi-anvil press with the Osugi-type guide block system (Ishii et al. 2016; 2019b) in combination with the same sample configuration as the 24-GPa experiment. To synthesize Cf-type phases in the $NaAlSiO_4$, $NaAlSiO_4$-$MgAl_2O_4$, $NaAlSiO_4$-

$MgAl_2O_4$-Fe_3O_4 systems, the starting mixtures were packed in Re-foil capsules. The hydrous sample was packed in a welded Pt-tube capsule with two Pt lids. Cr-doped MgO octahedral pressure media with a 10-mm or 7-mm edges were used for experiments at 23 and 24 GPa in combination with tungsten carbide anvils with a 4- and 3 mm truncation, respectively. The detailed descriptions of cell assemblies were reported in Kawazoe et al. (2017) and Liu et al. (2020), respectively. The sample was first compressed to a desired press load corresponding to 23-24 GPa (Keppler and Frost 2005) or 26 GPa (Liu et al. 2017), and then heated to 1100-2200 °C at 100 °C/min. After keeping the target temperature for the desired time (Table 1), the sample was quenched by cutting electrical power supply and decompressed to room pressure for 12-15 h.

The recovered samples were characterized by microfocus powder X-ray diffraction (XRD) for phase identification, single crystal XRD for structure refinement, electron microprobe analysis (EPMA) and Mössbauer spectroscopy for chemical analysis, and scanning electron microscopy for textual observation. Detailed general analytical are shown in the supplementary text in Online Material. EPMA measurements of the samples were generally performed at an accelerating voltage and probe current of 15 kV and 5 nA, respectively, for acquisition times of 10 s, except for run products from H5469, H5477 and S7759, which were measured for 5, 10 and 20 s each to examine whether their Na contents changed by Na volatilization. High-quality crystals of Cf-type phases with no inclusion and sharp optical extinction checked under a polarizing microscope were analyzed by single-crystal XRD. The analysis of systematic absences confirmed that all crystals were compatible with the space group *Pbnm* (#62). The structures of each sample were solved with the dual space algorithm *SHELXT* (Sheldrick, 2015a) and structural refinements were performed against F^2 using *SHELXL* in the the *Shelxle* GUI (Sheldrick, 2015b, Hübschle et al., 2011) employing atomic scattering factors for all atoms. We adopted two strategies to determine the element distribution over the three distinct cation sites of the Cf-type phase structure by single crystal XRD: (1) the distribution of the cations over the A, B1 and B2 site was inferred from the abundance of end-member components obtained from chemical analysis, assuming a random distribution of Al and Si the two octahedral sites (B1 and B2); (2) the fraction of each atom in the A, B1 and B2 sites was refined using chemical restraints based on compositional data from EPMA measurements. Detailed analytical methods are described in deposited CIF. In the final steps of each refinement, atomic positions and anisotropic displacement parameters were refined for

This is the peer-reviewed, final accepted version for American Mineralogist, published by the Mineralogical Society of America.
The published version is subject to change. Cite as Authors (Year) Title. American Mineralogist, in press.
DOI: https://doi.org/10.2138/am-2022-8748. http://www.minsocam.org/

all atoms, yielding crystallographic discrepancy factors (R1) of 3-4% (Table OM4), indicating that all the refinements were well converged. Because the results using both the strategies provide similar discrepancy factors and structural data (see deposited CIF), we will limit our discussion of structural data to the results obtained with the second strategy.

RESULTS AND DISCUSSION

Syntheses and characterization of Cf single crystals

Table 1 summarizes synthesis experiments in this study. Three runs were carried out to synthesize Cf-type $NaAlSiO_4$ at 23-26 GPa and 1700-2200 °C. All run products were identified as Cf-type phase. Single crystals with dimensions up to 100 μm were obtained only at 23 GPa and 2200 °C (Fig. OM1), while below this temperature the grain sizes were typically very small (~5-10 μm). One experiment at 23 GPa and 2000 °C was performed to synthesize Cf-type single crystals along the $NaAlSiO_4$-$MgAlSiO_4$ join. The recovered crystals had dimensions up to 150 μm, although the presence of Re inclusions prevented us from using the largest ones for single-crystal X-ray diffraction analyses. Two runs at 23 GPa and 2000 °C were carried out to synthesize Cf-type phase in the $NaAlSiO_4$-$MgAl_2O_4$-Fe_3O_4 system, recovering crystals with dimensions up to 100-150 μm (Fig. 1a). No Cf-type phase was appeared in the hydrous conditions (Figs. OM3 and 4) due to the strong partitioning of Na into hydrous melt (Table OM2).

The compositions of the recovered crystals obtained from EPMA are $Na_{0.90(1)}Al_{1.03(2)}Si_{1.00(2)}O_4$, $Na_{0.66(4)}Mg_{0.28(4)}Al_{1.22(3)}Si_{0.78(3)}O_4$ $Na_{0.59(2)}Mg_{0.20(1)}Fe_{0.22(1)}Al_{1.28(2)}Si_{0.67(2)}O_4$ and $Na_{0.62(2)}Mg_{0.19(5)}Fe_{0.25(1)}Al_{1.20(3)}Si_{0.78(3)}O_4$ for H5477, S7759, H5469, and S7760, respectively (Table OM1). Note that cation vacancies were detected in all samples and are likely to be localized in the A site since the sum of Si, Al and Fe^{3+} is greater than 2 and thus can fully occupy the octahedral B1 and B2 sites. Mössbauer spectra of two Fe-bearing Cf crystals were fit using two doublets with hyperfine parameters compatible with 6-fold coordinated Fe^{3+} and 8-fold coordinated Fe^{2+}. The H5469 sample has 32(1)% of Fe^{3+} with QS = 0.74(2) mm/s and CS = 0.32(2) mm/s and remaining Fe^{2+} with QS = 3.31(1) mm/s and CS = 1.22(1) mm/s (Fig. 1b). On the other hand, the S7760 sample has 34(1)% of Fe^{3+} with quadrupole splitting (QS) = 0.74(2) mm/s and center shift (CS) = 0.33(1)

mm/s and remaining Fe^{2+} with QS = 3.34(1) mm/s and CS = 1.23(1) mm/s (Fig. OM2). These values are in excellent agreement with one another and are similar to those reported in Wu et al. (2017).

From our structural analysis of Cf-type crystals, we refined the site occupancy factors for all atomic species in the A, B1 and B2 sites. B1 generally shows higher Si contents than the B2 in all samples, while larger cations (i.e., Al, Fe^{3+}) seem to partition preferentially in the B2 site. This observation is in agreement with the refined interatomic octahedral distances, with the B2 site having consistently larger B-O distances than the B1 site. Additionally, the average B-O distances increase with increasing Al and Fe^{3+} content and are 1.862(2) and 1.870(2) Å in H5477, 1.869(2) and 1.883(2) Å in S7759, and 1.874(2) and 1.891(2) Å in H5460 for the B1 and B2 sites, respectively (Table OM6).

By refining the site occupancy factors of cations in the A site, the number of vacancies in all samples and the site partitioning of Fe in H5469 can also be estimated. In the Fe-free H5477 and S7759 samples, vacancies amount to about 0.03 (Table OM5), which is significantly less than the values of about 0.06 obtained from EPMA. At the same time, the refined Na concentration in the A site is larger than that obtained from chemical analyses. We examined possible Na loss due to beam damage during EPMA measurements by varying the acquisition time for all elements between 5 s and 20 s. However, no systematic variation in the Na_2O concentration was observed (Table OM3). In the case of sample H5469, the concentrations of vacancies obtained from EPMA data and site occupancies from the structural refinement resulted consistent with one another. However, in this case, the refined Fe and Na contents in the A site resulted to be higher and lower, respectively, than what expected from chemical analyses, possibly because the two site occupancy factors were found to be highly correlated in the structural refinement. The average A-O interatomic distance for H5477 is 2.348(2) Å (Table OM 6), which is slightly shorter than that of 2.397 Å in $NaAlSiO_4$ composition determined by Rietveld analysis of powdered samples (Yamada et al., 1983). This further supports that the Cf-type phase synthesized in this study has both vacancies and aluminum in the 8-fold coordinated A site. Yamada et al. (1983) synthesized Cf-type $NaAlSiO_4$ at 24-30 GPa and 1000-1200 °C. The relatively low-temperature synthesis conditions may have

prevented the formation of vacancy, although no compositional analysis was conducted on the recovered sample. The average interatomic distance in samples S7759 and H5469 has values of 2.324(2) and 2.325(2) Å (Table OM 6), which is less than observed in Fe,Mg-free samples of H5477, suggesting that the average A-O distance in Cf-type aluminous phases increases with increasing Na content.

Molar volume systematics of Cf-type phases

The molar volumes of Cf-type solid solutions as a function of $Na/(Na+Mg+Fe^{2+})$ is shown in Figure 3. The molar volume of the end-member $NaAlSiO_4$ component determined in this study is in good agreement with those determined in previous studies by powder X-ray diffraction (Guignot & Andrault, 2004; Tutti et al., 2000; Yamada et al., 1983), despite the higher concentration of cation vacancies. Molar volumes of Mg-bearing samples synthesized in this study and in the previous study of Ono et al (2009) lie respectively below and above the trend that would be expected for a linear mixing behavior with Cf-type $MgAl_2O_4$ (Funamori et al., 1998; Irifune et al., 1991; Kojitani et al., 2007; Stixrude & Lithgow-Bertelloni, 2022). Based on our observation on the end-member $NaAlSiO_4$, the presence of few-percent cation vacancy components (i.e. $\square Si_2O_4$, $\square Al_{8/3}O_4$) seems to have a negligible effect on the molar volume of Cf-type phase. Therefore, the observed discrepancy with the sample of Ono et al. (2009) lies either in the higher Si content in the octahedral sites of our sample (i.e. ~0.40 vs ~0.35, respectively) or in a non-linear effect of cation vacancy components with composition, although the latter option seems less likely. Fe incorporation in Cf-type phase, on the other hand, has a more pronounced effect and significantly increases the molar volume of Cf-type samples. Small amounts of octahedrally coordinated Fe^{3+} in the B sites appear to increase significantly the molar volume with respect to $NaAlSiO_4$, given that the ionic radius of $^{VI}Fe^{3+}$ is about 20% larger than $^{VI}Al^{3+}$ and 60% larger than $^{VI}Si^{4+}$ (Shannon, 1976). Nonetheless, the molar volume of H5469 plots below the linear extrapolation between $NaAlSiO_4$ and the $Fe^{2+}Al_2O_4$ end member which has been studied only by computational methods (Stixrude and Lithgow-Bertelloni, 2022). This suggests that either the molar volume of $Fe^{2+}Al_2O_4$ is actually lower than previously proposed or that the mixing behavior between $NaAlSiO_4$ and $Fe^{2+}Al_2O_4$ strongly deviates from linearity. Large excess molar properties, such as the excess molar

volume, are to be expected when an end-member component of a given solid solution is not thermodynamically stable, which was suggested to be the case of $Fe^{2+}Al_2O_4$ with Cf-type structure (Schollenbruch et al., 2010). In either case, more extensive experimental work is needed to better constrain the molar volume of solid solutions with Cf-type structure along the $NaAlSiO_4$-$Fe^{2+}Al_2O_4$ join.

IMPLICATIONS

The present synthesized samples under dry conditions and their single-crystal X-ray diffraction analyses indicate that the Cf-type phases in basaltic compositions are stable at least around 660 km depths and up to 2200 °C. It was shown that Cf-type $MgAl_2O_4$ may become unstable and transform to a $CaTi_2O_4$ (Ct) -type phase, which also exhibits double chains of octahedral B-sites but with a different vertex-sharing framework, resulting in the *Cmcm* space group (Ishii et al. 2018), in upwelling hot plume at topmost lower mantle pressures (Ishii et al., 2021). The wider stability of $NaAlSiO_4$-rich Cf phases might be because the 8-fold coordinated site in the Ct-type structure, which is essentially a prism site (Ishii et al. 2014. 2015, 2018), is too tight to accommodate Na cations.

Previous phase-relation studies of a hydrous basaltic crust composition showed that Al-rich phase D and phase δ-H coexist with stishovite, davemaoite and bridgmanite/garnet at 23-26 GPa and 1000-1200 °C (Liu et al., 2019). No Cf-type phase was observed, likely due to the formation of Al-rich hydrous phases and Na-rich melt. Our study thus showed that hydrous conditions are not suitable for the synthesis of Cf-type phases even at higher temperatures, where Al-rich hydrous phases are not stable, because of the strong partitioning of Na into hydrous melt.

We have better constrained the defect chemistry of Cf phase at 23 GPa, corresponding to ~660 km depth, by combining EPMA and single crystal XRD, showing that some A-site vacancies are likely present in the crystal structure. Although electrical conduction mechanism and element diffusion rates in the Cf phase have not been investigated yet, the Cf phase may have relatively high electrical conductivity and low viscosity compared with other mantle minerals due to some A-site vacancies. In this case, these properties can contribute to electrical conductivity increase and viscosity decrease at least below 660 km depth (e.g., Civet et al.

2015; Rudolph et al. 2015). Further studies on the defect chemistry of Cf phases at higher pressures and direct measurements of mentioned physical properties will help to pinpoint the role of this phase in the lower mantle dynamics.

The present study suggests that accurate chemical and structural characterization is essential to accurately model the physical properties of Cf-type phases. Previous studies investigated compressibility of $NaAlSiO_4$, $MgAl_2O_4$ and $Na_{0.88}Al_{0.99}Fe_{0.13}Si_{0.94}O_4$ ($Fe^{3+}/\Sigma Fe$ = 90%) (Dubrovinsky et al. 2002; Sueda et al. 2009; Wu et al. 2017, respectively). Dai et al. (2013) measured the shear wave velocity of $Na_{0.4}Mg_{0.6}Al_{1.6}Si_{0.4}O_4$ at high pressure by means of Brillouin scattering on a powdered sample. Compositions of Fe-bearing Cf-type phases with $Fe^{3+}/\Sigma Fe$ = 0.32-0.34 synthesized in the present study are quite close to those in a basaltic crust composition ($Fe^{3+}/\Sigma Fe$ ~ 0.1-0.2, Ishii et al., 2022). Our single-crystal structural analyses also suggested that not all of Fe^{3+} is in octahedral coordination. This means that a high-to-low spin crossover of octahedrally coordinated Fe^{3+} in Cf-type phase at lower mantle pressures will likely have more limited effects on the elastic and transport properties of a basaltic phase assemblage than it would be expected for Fe^{3+}-rich phases (e.g., Hsieh et al., 2020, 2022; Wu et al., 2017). Large and homogeneous single crystals synthesized in this study are therefore ideal to test these hypotheses through high-pressure studies and will enable to better constrain the physical properties of dry basaltic crust at lower mantle conditions.

ACKNOWLEDGMENTS

We thank H. Fischer and R. Njul for the preparation of cell assemblies and sample preparation for SEM and EPMA measurements, respectively. This work was supported by the National Natural Science Foundation of China, the National Key Research Major Research Plan on West-Pacific Earth System Multispheric Interactions (92158206 to R. Tao and T.I.). We also thank one anonymous reviewer for constructive comments.

REFERENCES CITED

Ballmer, M. D., Schmerr, N. C., Nakagawa, T., and Ritsema, J. (2015). Compositional mantle layering revealed by slab stagnation at ~1000-km depth. Science Advances. 1, e1500815.

Civet, F., Thébault, E., Verhoeven, O., Langlais, B., and Saturnino, D. (2015). Electrical conductivity of the Earth's mantle from the first Swarm magnetic field measurements. Geophysical Research Letters, 42, 3338-3346.

Dubrovinsky, L. S., Dubrovinskaia, N. A., Prokopenko, V. B., and Le Bihan, T. (2002). Equation of state and crystal structure of $NaAlSiO_4$ with calcium-ferrite type structure in the conditions of the lower mantle. High Pressure Research, 22, 495-499.

Funamori, N., Jeanloz, R., Nguyen, J. H., Kavner, A., Caldwell, W. A., Fujino, K., Miyajima, N., Shinmei, T., and Tomioka, N. (1998). High-pressure transformations in $MgAl_2O_4$. Journal of Geophysical Research: Solid Earth, 103, 20813-20818.

Guignot, N., and Andrault, D. (2004). Equations of state of Na–K–Al host phases and implications for MORB density in the lower mantle. Physics of the Earth and Planetary Interiors, 143, 107-128.

Hsieh, W. P., Ishii, T., Chao, K. H., Tsuchiya, J., Deschamps, F., and Ohtani, E. (2020). Spin transition of iron in δ-(Al,Fe)OOH induces thermal anomalies in Earth's lower mantle. Geophysical Research Letters, 47, e2020GL087036.

Hsieh, W. P., Marzotto, E., Ishii, T., Dubrovinsky, L., Aslandukova, A. A., Criniti, G., Y.C., Tsao, C.H., Lin, J., Tsuchiya, and Ohtani, E. (2022). Low thermal conductivity of hydrous phase D leads to a self-preservation effect within a subducting slab. Journal of Geophysical Research: Solid Earth, e2022JB024556.

Hübschle, C. B., Sheldrick, G. M., and Dittrich, B. (2011). ShelXle: a Qt graphical user interface for SHELXL. Journal of applied crystallography, 44, 1281-1284.

Ishii, T., Kojitani, H., Tsukamoto, S., Fujino, K., Mori, D., Inaguma, Y., Tsujino, N., Yoshino, T., Yamazaki, D., Higo, Y., Funakoshi, K., and Akaogi, M. (2014). High-pressure phase transitions in $FeCr_2O_4$ and structure analysis of new post-spinel $FeCr_2O_4$ and $Fe_2Cr_2O_5$ phases with meteoritical and petrological implications. American Mineralogist, 99, 1788-1797.

Ishii, T., Kojitani, H., Fujino, K., Yusa, H., Mori, D., Inaguma, Y., Matsushita, Y., Yamaura, K., and Akaogi, M. (2015). High-pressure high-temperature transitions in $MgCr_2O_4$ and crystal structures of new $Mg_2Cr_2O_5$ and post-spinel $MgCr_2O_4$ phases with implications for ultrahigh-pressure chromitites in ophiolites. American Mineralogist, 100, 59-65.

Ishii, T., Shi, L., Huang, R., Tsujino, N., Druzhbin, D., Myhill, R., Li, Y., Lin, W., Yamamoto, T., Miyajima, N., Kawazoe, T., Nishiyama, N., Higo, Y., Tange, Y., and Katsura, T. (2016). Generation of pressures over 40 GPa using Kawai-type multi-anvil press with tungsten carbide anvils. Review of Scientific Instruments, 87, 024501.

Ishii, T., Sakai, T., Kojitani, H., Mori, D., Inaguma, Y., Matsushita, Y., Yamaura, K., and Akaogi, M. (2018). High-pressure phase relations and crystal structures of postspinel phases in MgV_2O_4, FeV_2O_4, and $MnCr_2O_4$: Crystal chemistry of AB_2O_4 postspinel compounds. Inorganic Chemistry, 57, 6648-6657.

Ishii, T., Kojitani, H., and Akaogi, M. (2019a). Phase relations of harzburgite and MORB up to the uppermost lower mantle conditions: precise comparison with pyrolite by multisample cell high-pressure experiments with implication to dynamics of subducted slabs. Journal of Geophysical Research: Solid Earth, 124, 3491-3507.

Ishii, T., Liu, Z., and Katsura, T. (2019b). A breakthrough in pressure generation by a Kawai-type multi-anvil apparatus with tungsten carbide anvils. Engineering, 5, 434-440.

Ishii, T., Criniti, G., Bykova, E., Dubrovinsky, L., Katsura, T., Arii, H., Kojitani, H., and Akaogi, M. (2021). High-pressure syntheses and crystal structure analyses of a new low-density $CaFe_2O_4$-related and $CaTi_2O_4$-type $MgAl_2O_4$ phases. American Mineralogist, 106, 1105-1112.

Ishii, T., Miyajima, N., Criniti, G., Hu, Q., Glazyrin, K., and Katsura, T. (2022). High pressure-temperature phase relations of basaltic crust up to mid-mantle conditions. Earth and Planetary Science Letters, 584, 117472.

Kaneshima, S. (2019). Seismic scatterers in the lower mantle near subduction zones. Geophysical Journal International, 219, S2-S20.

Kawazoe, T., Ohira, I., Ishii, T., Boffa Ballaran, T., McCammon, C., Suzuki, A., and Ohtani, E. (2017). Single crystal synthesis of δ-(Al,Fe)OOH. American Mineralogist, 102, 1953-1956.

Keppler, H., and Frost, D.J. (2005) Introduction to minerals under extreme conditions. In R. Miletich, Ed., Mineral Behaviour at Extreme Conditions. EMU Notes in Mineralogy, 7, 1–30.

Kojitani, H., Hisatomi, R., and Akaogi, M. (2007). High-pressure phase relations and crystal chemistry of calcium ferrite-type solid solutions in the system $MgAl_2O_4$-Mg_2SiO_4. American Mineralogist, 92, 1112-1118

Liu, Z., Nishi, M., Ishii, T., Fei, H., Miyajima, N., Ballaran, T. B., Ohfuji, H., Sakai, T., Wang, L., Shcheka, S., Arimoto, T., Tange, Y., Higo, Y., Irifune, T., and Katsura, T. (2017). Phase relations in the system $MgSiO_3$-Al_2O_3 up to 2300 K at lower mantle pressures. Journal of Geophysical Research: Solid Earth, 122, 7775-7788.

Liu, Z., McCammon, C., Wang, B., Dubrovinsky, L., Ishii, T., Bondar, D., Nakajima, A., Tange, Y., Higo, Y., Cui, T., Liu, B., and Katsura, T. (2020). Stability and solubility of the $FeAlO_3$ component in bridgmanite at uppermost lower mantle conditions. Journal of Geophysical Research: Solid Earth, 125, e2019JB018447.

Liu, X., Matsukage, K. N., Nishihara, Y., Suzuki, T., and Takahashi, E. (2019). Stability of the hydrous phases of Al-rich phase D and Al-rich phase H in deep subducted oceanic crust. American Mineralogist, 104, 64-72.

Momma, K., and Izumi, F. (2011). VESTA 3 for three-dimensional visualization of crystal, volumetric and morphology data. Journal of Applied Crystallography, 44, 1272-1276.

Ono, A., Akaogi, M., Kojitani, H., Yamashita, K., and Kobayashi, M. (2009). High-pressure phase relations and thermodynamic properties of hexagonal aluminous phase and calcium-ferrite phase in the systems $NaAlSiO_4$–$MgAl_2O_4$ and $CaAl_2O_4$–$MgAl_2O_4$. Physics of the Earth and Planetary Interiors, 174, 39-49.

Rudolph, M. L., Lekić, V., and Lithgow-Bertelloni, C. (2015). Viscosity jump in Earth's mid-mantle. Science, 350, 1349-1352.

Satta, N., Criniti, G., Kurnosov, A., Boffa Ballaran, T., Ishii, T., & Marquardt, H. (2021). High-Pressure Elasticity of δ-(Al, Fe) OOH Single Crystals and Seismic Detectability of Hydrous MORB in the Shallow Lower Mantle. Geophysical Research Letters, 48, e2021GL094185.

Schollenbruch, K., Woodland, A. B., and Frost, D. J. (2010). The stability of hercynite at high pressures and temperatures. Physics and Chemistry of Minerals, 37, 137-143.

Shannon, R. D. (1976). Revised effective ionic radii and systematic studies of interatomic distances in halides and chalcogenides. Acta crystallographica section A: crystal physics, diffraction, theoretical and general crystallography, 32, 751-767.

Sheldrick, G. M. (2015a). Crystal structure refinement with SHELXL. Acta Crystallographica Section C: Structural Chemistry, 71, 3-8.

Sheldrick, G. M. (2015b). SHELXT–Integrated space-group and crystal-structure determination. Acta Crystallographica Section A: Foundations and Advances, 71, 3-8.

Stixrude, L., and Lithgow-Bertelloni, C. (2022). Thermal expansivity, heat capacity and bulk modulus of the mantle. Geophysical Journal International, 228, 1119-1149.

Sueda, Y., Irifune, T., Sanehira, T., Yagi, T., Nishiyama, N., Kikegawa, T., and Funakoshi, K. I. (2009). Thermal equation of state of $CaFe_2O_4$-type $MgAl_2O_4$. Physics of the Earth and Planetary Interiors, 174, 78-85.

Tutti, F., Dubrovinsky, L. S., and Saxena, S. K. (2000). High pressure phase transformation of jadeite and stability of $NaAlSiO_4$ with calcium-ferrite type structure in the lower mantle conditions. Geophysical Research Letters, 27, 2025-2028.

Wu, Y., Qin, F., Wu, X., Huang, H., McCammon, C. A., Yoshino, T., Zhai, S., Xiao, Y., and Prakapenka, V. B. (2017). Spin transition of ferric iron in the calcium-ferrite type aluminous phase. Journal of Geophysical Research: Solid Earth, 122, 5935-5944.

Yamada, H., Matsui, Y., and Ito, E. (1983). Crystal-chemical characterization of $NaAlSiO_4$ with the $CaFe_2O_4$ structure. Mineralogical Magazine, 47, 177-181.

FIGURE CAPTIONS

Figure 1. (a) A photograph of Fe-bearing $NaAlSiO_4$-$MgAl_2O_4$ (H5469) calcium ferrite single-crystals. (b) A Mössbauer spectrum of recovered Fe-bearing calcium ferrite sample (H5469). CS, center shift; QS, quadrupole splitting. (c) The crystal structure of the recovered sample (H5469). Different color areas in the spheres of A, B1 and B2 sites show the ratio of constituent atoms. □: vacancy. The crystal structure was drawn with the VESTA software (Momma and Izumi, 2011).

Figure 2. Molar volume variation of Cf-type phases as a function of the Na content in the 8-fold coordinated A site. Dashed lines represent the mixing behavior expected for an ideal solid solution using the end-member volumes reported in Stixrude and Lithgow-Bertelloni (2022). Error bars are smaller than the symbol when they are not shown.

Table 1. Experimental conditions, phase assemblages, and crystal sizes of calcium ferrite phases.

This is the peer-reviewed, final accepted version for American Mineralogist, published by the Mineralogical Society of America.
The published version is subject to change. Cite as Authors (Year) Title. American Mineralogist, in press.
DOI: https://doi.org/10.2138/am-2022-8748. http://www.minsocam.org/

Run no.	Starting material	P	T	D	Phases	Cf crystal size[a]
		GPa	°C	h		μm
H5477	Np	23	2200	2	Cf	100
I1195	Np	26	1700	4	Cf	5
S7759	Np	23	2000	2	Cf	10
	80Np-20Sp	23	2000	2	Cf	150
S7760	70Np-20Sp-10Mg	23	2000	2	Cf	100
H5469	70Np-20Sp-10Mg	23	2000	2	Cf	150
H5474	70Np-20Sp-10Mg+H_2O	24	1100	5	δ-H+ε-H+St+L	-
H5462	70Np-20Sp-10Mg+H_2O	24	1700	4	Cor+St+L+LN	-
H5471	70Np-20Sp-10Mg+H_2O	24	2000	3.5	Cor+St+L	-

Np, $NaALSiO_4$ nepheline; Sp, $MgAl_2O_4$ spinel; Mg, Fe_3O_4 magnetite; Cf, calcium ferrite phase, δ-H, AlOOH-rich hydrous phase δ-H; ε-H, FeOOH-rich hydrous phase ε-H; St, stishovite; Cor, corundum; L, melt.

[a]Maximum dimension

This is the peer-reviewed, final accepted version for American Mineralogist, published by the Mineralogical Society of America.
The published version is subject to change. Cite as Authors (Year) Title. American Mineralogist, in press.
DOI: https://doi.org/10.2138/am-2022-8748. http://www.minsocam.org/

Figure 1

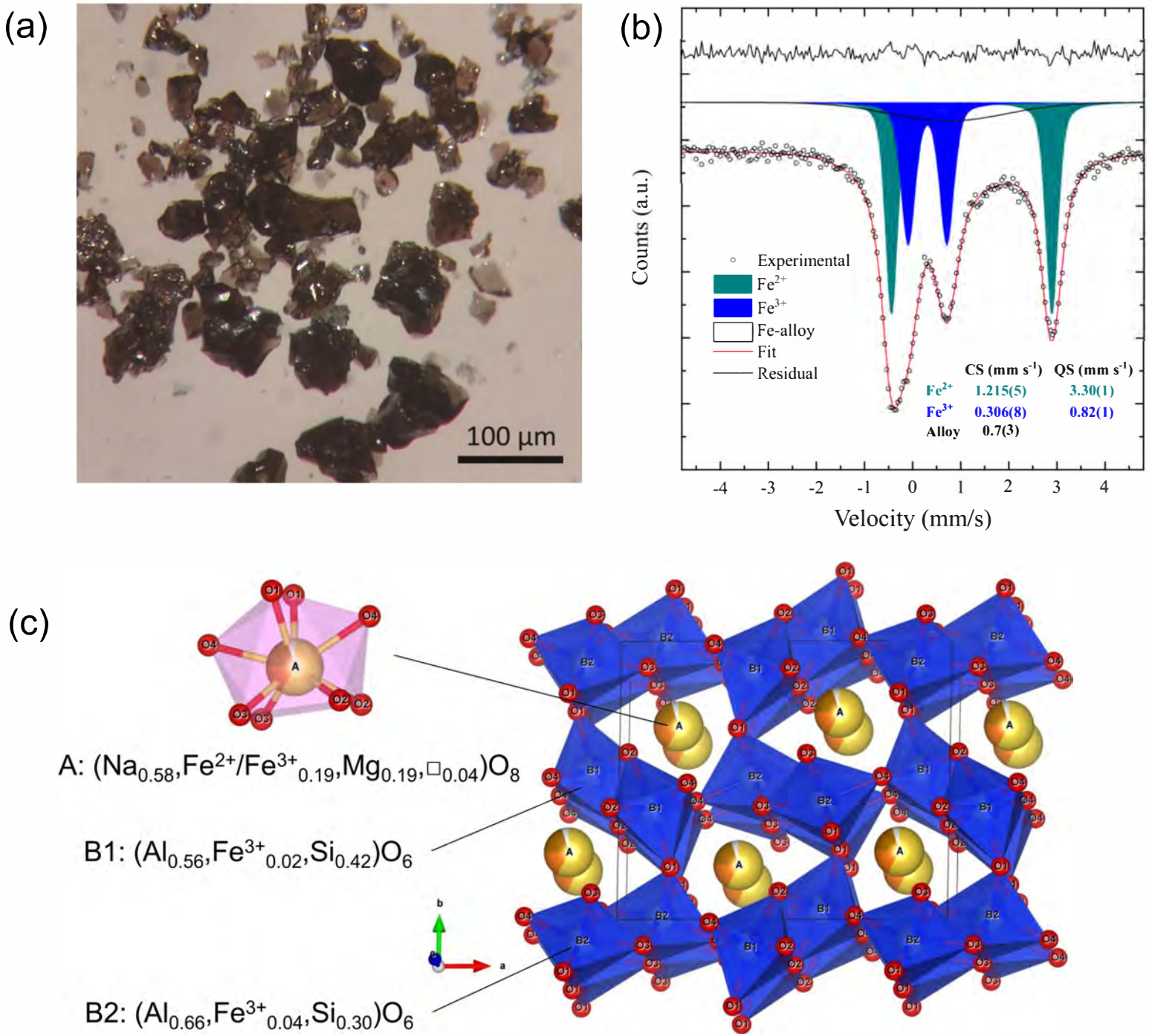

This is the peer-reviewed, final accepted version for American Mineralogist, published by the Mineralogical Society of America.
The published version is subject to change. Cite as Authors (Year) Title. American Mineralogist, in press.
DOI: https://doi.org/10.2138/am-2022-8748. http://www.minsocam.org/

Figure 2